scientific reports

Check for updates

OPEN

Study of morphology, phase composition, optical properties, and thermal stability of hydrothermal zirconium dioxide synthesized at low temperatures

Yuriy Garanin[1,2]✉, Rafael Shakirzyanov[1,2], Daryn Borgekov[1,2], Artem Kozlovskiy[1,2], Natalia Volodina[1], Dmitriy Shlimas[1,2] & Maxim Zdorovets[1,2]

Oxide nanoparticles exhibit unique features such as high surface area, enhanced catalytic activity, and tunable optical and electrical properties, making them valuable to various industry applications as well as for the development of new research projects. Nowadays, ZrO_2 nanoparticles are widely used as catalysts and precursors in ceramic technology. Hydrothermal synthesis with metal salts is one of the most common methods for producing stable tetragonal-phase zirconium dioxide nanoparticles. However, hydrothermal synthesis requires relatively high process temperatures (160–200 °C) and the use of advanced heat-resistant autoclaves capable of maintaining high pressure. This paper investigates how different precursors ($ZrOCl_2{\cdot}8H_2O$ and $ZrO(NO_3)_2{\cdot}2H_2O$) and synthesis temperatures (110–160 °C) affect the phase composition, optical properties, size, and shape of ZrO_2 nanoparticles produced by hydrothermal synthesis without calcination. In addition, the effect of temperature exposure in the range of 100–1000 °C on the phase stability of the synthesized nanoparticles was studied. X-ray diffraction and Raman spectroscopy techniques were used to determine the structure and phase composition, while the optical properties were examined through the analysis of transmission and absorption spectra in the visible and UV ranges. It was found that the obtained particles at synthesis temperatures of 110–130 °C have predominantly cubic c-ZrO_2 phase, which changes to monoclinic phase when heated above 500 °C. Analysis of visible and UV spectroscopy data reveals that the experimental samples have pronounced absorption in the middle UV range (200–260 nm) and have an energy band gap E_g varying from 4.8 to 5.1 eV. The hydrothermal powders synthesized in this study can be used as absorbers in the mid-UV range and as reinforcing additives in the preparation of technical ceramics.

Keywords Hydrothermal synthesis, ZrO_2, Phase transformation, Optical properties, Temperature stability

Zirconium dioxide (ZrO_2) has unique properties such as high values of mechanical strength, fire resistance, low chemical activity, high ionic conductivity, and low thermal conductivity at high temperatures. Due to these characteristics, ZrO_2 is a promising material across various fields of science and industry[1–3]. In particular, ZrO_2 is used as a material for oxidizing diesel soot[4], in optoelectronics[5], as electrodes and electrolytes in solid oxide fuel cells (SOFCs)[6], in dentistry[7], as catalysts for water splitting[8], and as a material for ultraviolet (UV) radiation absorption[9–12]. ZrO_2 at normal pressure, depending on the temperature, has three different crystal structures: (1) monoclinic (m-ZrO_2), at temperatures up to 1175 ℃; (2) tetragonal (t-ZrO_2), at temperatures from 1175 to 2370 ℃; (3) cubic (c-ZrO_2), at temperatures from 2370 to 2680 ℃[13]. Most of the above-mentioned unique properties are characteristic of the tetragonal and cubic phases of zirconium dioxide. Thus, t-ZrO_2 has high fracture toughness, catalytic activity and biocompatibility[14,15], due to which t-ZrO_2 is used as a reinforcing additive in Al_2O_3 ceramics. Also, stabilized tetragonal zirconia can be considered as a promising biomaterial[16,17]. At the same time, c-ZrO_2 has high oxygen conductivity and chemical stability at high temperatures and pressures[18,19], which

[1]Engineering Profile Laboratory, L.N. Gumilyov Eurasian National University, Satpayev St., Astana 010008, Kazakhstan. [2]Laboratory of Solid State Physics, The Institute of Nuclear Physics, Almaty 050032, Kazakhstan. ✉email: garanin_yua_1@enu.kz

allows it to be used as cathodes in solid fuel oxide elements and heat-resistant ceramics[20,21]. The stabilization of these phases is a key focus for materials scientists working with zirconia ceramics, refractory coatings, catalysts, and nanoparticles. High-temperature t-ZrO_2 and c-ZrO_2 polymorphs exist at room temperature if doped with additives such as Y_2O_3, CaO, CeO_2, and MgO[22–25]. When the Zr^{4+} cation is substituted with a cation of a different ionic radius, such as Y^{3+}, Mg^{2+}, Ca^{2+}, or Ce^{4+}, the reverse martensitic transformation from t-ZrO_2 and c-ZrO_2 to m-ZrO_2 does not occur[26]. This substitution prevents the shear displacement of zirconium cations and oxygen anions, thereby preventing the phase transition during cooling. Another method to achieve high-temperature phases is to obtain ZrO_2 particles with a size of 20 nm or less. The metastable t-ZrO_2 and c-ZrO_2 phases in the synthesized particles can be stabilized due to the high surface energy of the nanoparticles[27–30].

Currently, ZrO_2 nanoparticles are produced using such methods as the sol–gel method, solvothermal, spray pyrolysis, green method, chemical vapor deposition (CVD), and hydrothermal synthesis[31,32]. Among the listed methods, hydrothermal synthesis is most commonly used to synthesize nanoparticles[33–35]. Hydrothermal synthesis is highly promising due to its simplicity, cost-effectiveness, and the ability to vary process parameters over a wide range, including synthesis temperature, solution pH, and the type of mineralizer used. In the hydrothermal method, the size (from nanometers to micrometers), shape of the particles, and their phase composition can be controlled. Many studies have reported the preparation of ZrO_2 nanoparticles using the hydrothermal method, achieving sizes ranging from a few to hundreds of nanometers with a well-controlled size distribution[27,36,37].

In the hydrothermal synthesis of ZrO_2 nanoparticles, several types of precursors are used. For example, Moshen et al.[33] used $ZrOCl_2$-$8H_2O$ as the raw material and varied the pH of the suspension by changing the content of NaOH mineralizer, resulting in ZrO_2 nanoparticles with partial t-ZrO_2 content. In addition, Shizhong Wang et al.[38] also obtained ZrO_2 nanoparticles with a partial content of metastable t-ZrO_2 by supercritical hydrothermal synthesis using $ZrO(NO_3)_2$-$2H_2O$ as a precursor. The fabrication of ZrO_2 nanoparticles by hydrothermal synthesis is mainly conducted at temperatures in the range of 160–250 ℃[28,33,36,39,40]. Reducing the process temperature in hydrothermal synthesis could be beneficial due to the lower production costs of nanoparticles.

In this work, the structure, morphology, temperature stability, and optical properties of ZrO_2 nanoparticles prepared by hydrothermal synthesis in the temperature range of 110–160 °C were studied. This range was chosen to investigate the possibility of lowering the synthesis temperatures of stabilized zirconium dioxide nanoparticles. A combination of X-ray diffraction and Raman spectroscopy techniques was used to study the crystal structure. The optical properties of the synthesized particles were studied for potential applications in ultraviolet absorption. The thermal stability of the particles was investigated to assess their potential use as a reinforcing additive in ceramics, such as zirconia toughened alumina (ZTA)[27]. Information on the temperature stability of the reinforcing particles is crucial to prevent issues such as unwanted phase transformations during the sintering of ceramic components. This is especially important for ZrO_2 particles due to the martensitic transition from t-ZrO_2 to c-ZrO_2, which is accompanied by a significant change in the lattice volume. These changes induce critical mechanical stresses in the ceramic microstructure, leading even to cracking of the sintered compacts. Thus, this study aims to provide essential data for the future application of ZrO_2 nanoparticles synthesized via the hydrothermal method.

Methods and materials

ZrO_2 nanoparticles were prepared using a hydrothermal synthesis method in a steel autoclave with a Teflon liner. The autoclave reactor volume was 25 mL, and the reactor was 90% full during synthesis. Zirconyl chloride octahydrate ($ZrOCl_2 \cdot 8H_2O$) (Sigma Aldrich, Saint Louis, USA) and zirconyl nitrate dihydrate ($ZrO(NO_3)_2 \cdot 2H_2O$) (Sigma Aldrich, Saint Louis, USA) were used as precursors. For each of the precursors, 17.5 mL of 0.1 mol/L zirconium salt solution in distilled water was prepared. To prevent the formation of particle conglomerates during synthesis, 0.14 g of polyethylene glycol 6000 (PEG 6000) was added to the solution. A 5 ml solution of 10 mol/L NaOH in distilled water was used as the mineralizer. The hydrothermal synthesis was conducted in the IKA OVEN 125 basic dry drying oven (IKA-Werke GmbH & CO. KG, Staufen, Germany) at temperatures ranging from 110 to 160 ℃, for 12 h under autogenous water vapor pressure. The reactor was cooled under atmospheric conditions in a turned-off drying oven. After synthesis, the particles were processed through centrifugation in distilled water and ethanol, followed by boiling in ethanol. Obtained particles were then filtered and dried in an oven at 50 °C.

X-ray diffraction analysis was performed using X-ray diffraction on a Bruker D8-advance diffractometer (Bruker GmbH, Mannheim, Germany) with Cu-K_α radiation in Bragg–Brentano geometry. The size of the coherent scattering region (CSR) was calculated for the (111) reflections of the monoclinic and cubic (or (101) for tetragonal) phases of ZrO_2. These reflections were initially approximated using the Pseudo–Voigt function with the Scherrer equation[41]:

$$d_{XRD} = \frac{0.9\lambda}{\beta cos\theta}, \tag{1}$$

where β is the width at half maximum (FWHM) for each of the reflections and 0.9 is a coefficient accounting for particle shape.

The fraction of monoclinic phase in the experimental samples was calculated using[42]:

$$\nu_m = \frac{1.311X_m}{1 + 0.311X_m}, \tag{2}$$

where

$$X_m = \frac{I_m\left(\bar{1}11\right) + I_m(111)}{I_m\left(\bar{1}11\right) + I_m\left(111\right) + I_c(111)} \tag{3}$$

where I_m and I_c are intensities of the corresponding reflections on the diffractogram.

The phase composition of the synthesized particles was also examined using Raman spectroscopy on an Enspectr M532 spectrometer (Spectr-M LLC, Chernogolovka, Russia) with a laser wavelength of 532 nm. The size and morphology of the obtained ZrO_2 particles were investigated using transmission electron microscopy (TEM) with a Jeol JEM—1400Plus transmission electron microscope (Jeol, Tokyo, Japan). Mass loss thermograms during heating were recorded using thermogravimetric analysis (TGA) with a Themys One (Setaram KEP Technology, Caluire, France). TGA was conducted in an argon atmosphere with a partial pressure of 0.5 Pa. The samples were heated from room temperature to 1000 ℃ at a heating rate of 10 ℃/min for each sample. The optical properties of the synthesized ZrO_2 nanoparticles were investigated by UV–visible spectroscopy on a SPECORD 200/210/250 PLUS (Analytik Jena, Jena, Germany). The energy band gap (E_g) values were estimated by generating Tauc plots[43]:

$$(\alpha h\upsilon)^2 = C\left(h\upsilon - E_g\right), \tag{4}$$

where C is a constant, α is absorbance, and $h\upsilon$ is photon energy.

The study of phase stability of ZrO_2 particles was performed by annealing at temperatures in the range of 100–1000 ℃ in the Nabertherm LHT 08/18 (Nabertherm GmbH, Lilienthal, Germany) furnace for 2 h for each cycle with a heating rate of 10 ℃/min with subsequent evaluation of diffractograms using expressions (2) and (3).

Results and discussion

Figure 1 shows X-ray diffraction patterns for ZrO_2 particles obtained at different temperatures by hydrothermal synthesis. The presented data indicate that, regardless of the precursor used, ZrO_2 particles synthesized at temperatures of 110–130 ℃ contain exclusively the c-ZrO_2 phase (PDF 01-071-6425) with space group Fm-3m (225) or the t-ZrO_2 phase (PDF 00-050-1089) with space group P42/nmc (137). Due to the structural similarities and the close proximity of the main reflections in the X-ray diffraction patterns, it is challenging to accurately distinguish between the t-ZrO_2 and c-ZrO_2 phases in the samples. With further increase of the synthesis temperature, peaks characteristic of m-ZrO_2 (PDF 00-065-0687) space group P21/a(14) appear on the diffractograms. As the synthesis temperature rises, the activity within the reactor intensifies, leading to the formation of m-ZrO_2. This phase transition is driven by a reduction in surface energy, which occurs as the average particle size exceeds the critical range of 10–20 nm.

Analysis of the average crystallite sizes for c (or t)—ZrO_2 phases (Fig. 2), calculated using the Scherrer equation, shows that the average value $d_{c\,(or\,t)}$ does not change when varying the synthesis parameters and ranges from 5 to 6 nm. At the same time, the d_m values for m-ZrO_2 are in the range of 17–32 nm, surpassing the critical size threshold for the existence of the cubic (or tetragonal) phase of ZrO_2. The data obtained suggest that the monoclinic phase forms when the critical particle size of ZrO_2 is exceeded, triggering the c (t)→m phase transition.It is worth noting that for the samples produced from $ZrOCl_2{\cdot}8H_2O$, the formation of m-ZrO_2 occurs at a lower synthesis temperature, which can be explained by the fact that zirconyl chloride has a lower degree of hydrolysis, which is correlated with a higher degree of dissociation of hydrochloric compounds, compared to

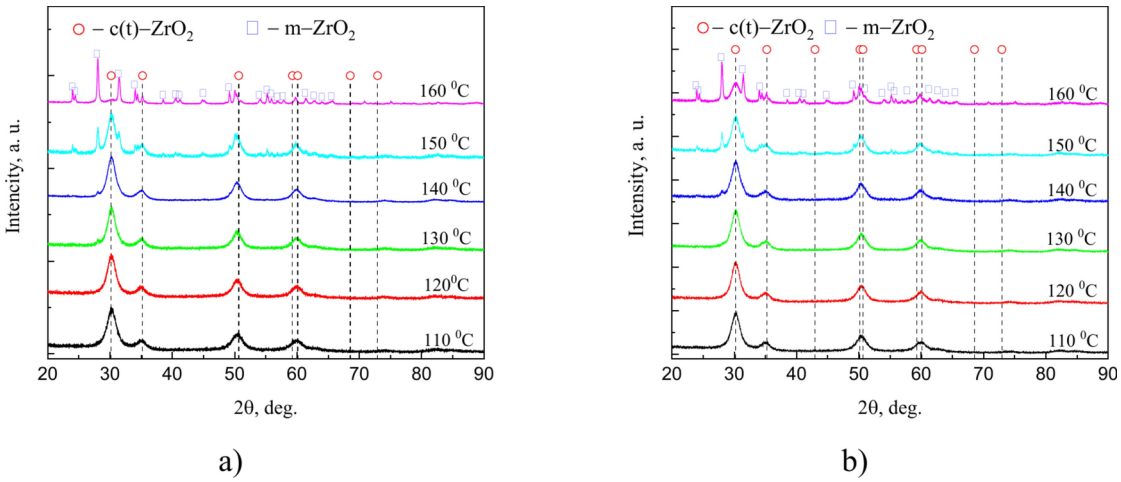

Fig. 1. X-ray diffractograms of ZrO_2 particles obtained using hydrothermal synthesis from (**a**) $ZrOCl_2{\cdot}8H_2O$ and (**b**) $ZrO(NO_3)_2{\cdot}2H_2O$ precursors at different temperatures.

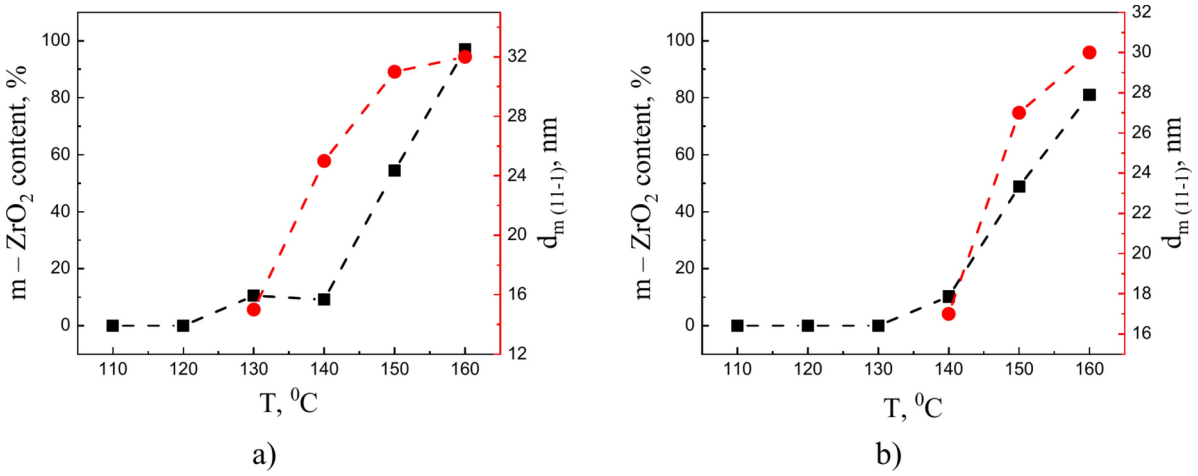

Fig. 2. Dependence of m-ZrO_2 phase content and $d_{(11-1)}$ for m-ZrO_2 nanoparticles, prepared from (**a**) $ZrOCl_2{\cdot}8H_2O$ and (**b**) $ZrO(NO_3)_2{\cdot}2H_2O$ on the hydrothermal synthesis temperature.

nitrate compounds[44]. As a result, ZrO_2 particles synthesized from $ZrOCl_2{\cdot}8H_2O$ at temperatures above 120 °C undergo sufficient growth, leading to a partial phase transition from c (or t)-ZrO_2 to m-ZrO_2.

Figures 3 and 4 show TEM images of synthesized ZrO_2 samples, from which it is clear that the obtained samples are spherical-shaped nanoparticles of 5–10 nm in size, forming larger conglomerates. The analysis of particle size distribution histograms reveals that as the synthesis temperature increases, the proportion of particles larger than 10 nm rises, with some particles eventually exceeding 100 nm (not shown in Figs. 3 and 4). This observation is consistent with the results calculated using the Debye–Scherrer equation.

Figure 5 demonstrates the change in particle shape from spherical to elongated "rod-like" for powders synthesized at 160 °C. The presence of cubic (or tetragonal) phase at high synthesis temperature is attributed to the preservation of some fraction of particles smaller than the critical size, which is confirmed by TEM images (Fig. 5b,d).

Raman spectroscopy is capable of distinguishing between the cubic and tetragonal phases of ZrO_2. Figure 6 illustrates the Raman spectra of the samples obtained using $ZrOCl_2{\cdot}8H_2O$ (6a) and $ZrO(NO_3)_2{\cdot}2H_2O$ (6b) as precursors at different temperatures. Samples synthesized at temperatures below 150 °C exhibit a broad peak around 600 cm^{-1}, which corresponds to the F_2g vibrational mode of cubic ZrO_2[45]. The modes at 273, 716, and 807 cm^{-1} characteristic of t-ZrO_2[24] are observed only for the sample synthesized at 140 ℃ for $ZrOCl_2{\cdot}8H_2O$ precursor. The presence of modes characteristic of the tetragonal phase may indicate the co-existence of t- and c-phases in the synthesized powders. From the analysis of Raman spectroscopy results, it can be stated that the particles contain predominantly c-ZrO_2 phase with a minor content of t-ZrO_2. When the synthesis temperature is above 130 ℃, the spectra show modes at 178, 190, 221, 308, 332, 346, 382, 477, 503, 538, 558, 612, and 630 $см^{-1}$ indicative of m-ZrO_2[45], which is consistent with the X-ray diffraction results.

Table 1 presents the data on the chemical composition of the samples obtained from different starting materials. As can be seen from the presented data, in addition to zirconium and oxygen, the chemical composition contains residues of synthesis products such as sodium, chlorine and nitrogen, which indicates the presence of residues of synthesis products.

When using ZrO_2 nanoparticles produced by hydrothermal synthesis as a precursor in the synthesis of high-density ceramics or as a reinforcing component, it is necessary to first remove physiosorbed and chemisorbed water as well as residual synthesis products (such as PEG and Na, Cl, N-containing compounds). Since the residual byproducts will be vaporized after pressing the green powder and subsequent sintering, the resulting volatile gases can create pores in the ceramics. TGA tests were conducted to investigate the mass loss and processes occurring to the particles during temperature exposure. The results for the sample obtained at 130 ℃ using $ZrOCl_2{\cdot}8H_2O$ and $ZrO(NO_3)_2{\cdot}2H_2O$ are shown in Fig. 7 (these curves were chosen as representative; similar curve trends were observed for the other samples). The curve can be divided into four distinct regions: (1) 100–200 °C, where the evaporation of physisorbed water from the particle surface occurs and decomposition of some residual synthesis products (such as NO_3) is possible; (2) 200–400 °C, which corresponds to the removal of chemisorbed water; (3) 400–600 °C, associated with the decomposition of hydroxyl (–OH) bonds; and (4) temperatures above 600 °C, where the decomposition of chemical compounds containing sodium, such as NaCl or $NaNO_3$, is observed.[29,33,46]. For all experimental samples, heating the particles to 1000 °C results in a mass loss of 14–17% of the initial weight, which is attributed to the removal of physisorbed and chemisorbed water, as well as –OH groups.

Figure 8 demonstrates the absorption spectra and Tauc plots of the energy band gap (E_g). For ZrO_2 nanoparticles obtained using $ZrOCl_2{\cdot}8H_2O$ and synthesis temperatures of 110–130 °C, a more pronounced absorption ability in the mid-UV range of 200–300 nm can be observed compared to other temperatures, as can be seen from the spectra of Fig. 8a. Table 2 presents the calculated energy bandgap E_g for ZrO_2 nanoparticles using Eq. (3). The E_g values for all samples are in the range of 4.89–5.09, which is in good agreement with

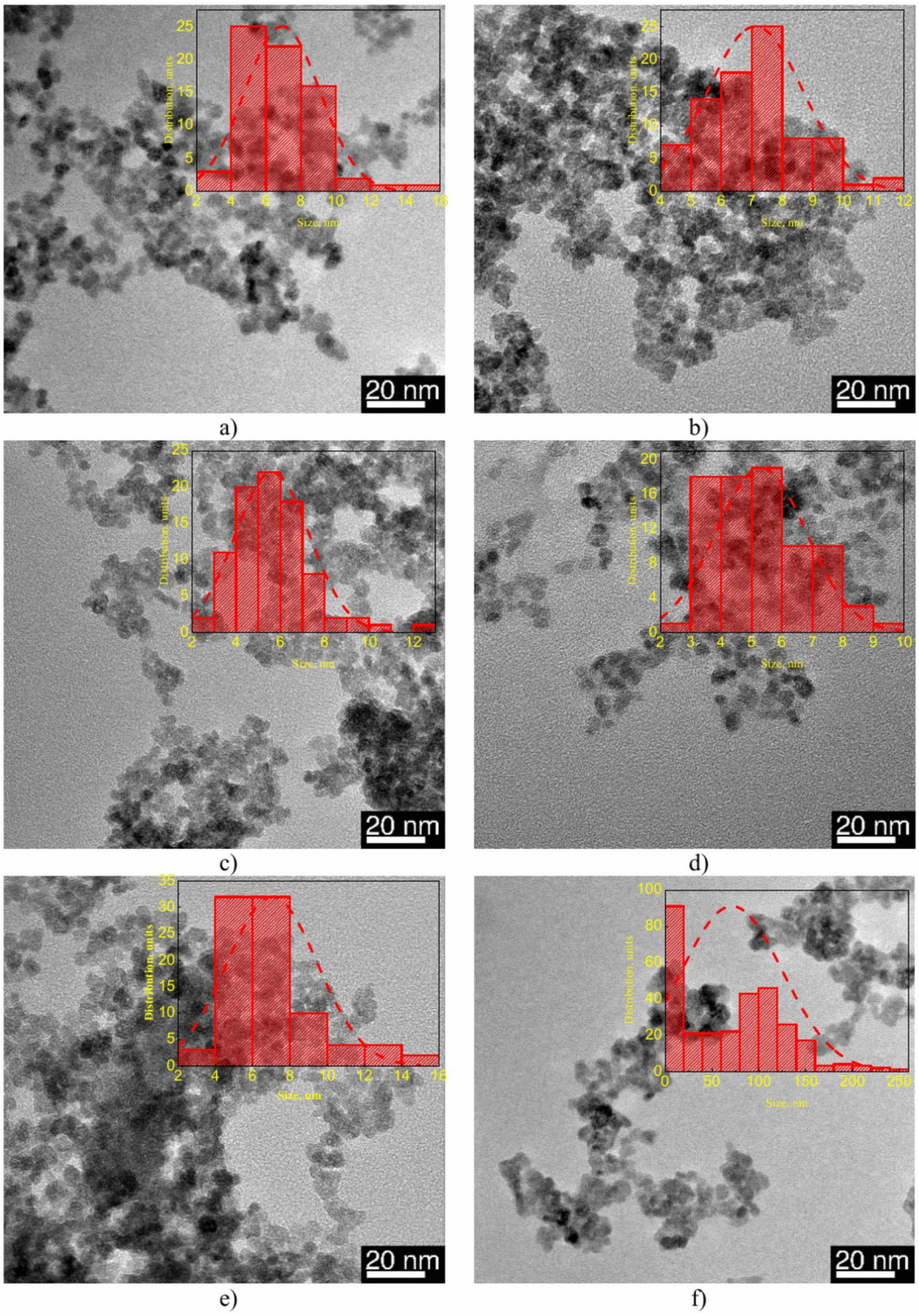

Fig. 3. TEM images of ZrO_2 particles obtained using $ZrOCl_2 \cdot 8H_2O$ by hydrothermal synthesis at temperatures (**a**–**f**) 110–160 °C.

the literature data[47]. No clear dependences between E_g values and the parameters of hydrothermal synthesis were found. A possible explanation for this fact could be the presence of chemisorbed and physisorbed water in the powders produced by hydrothermal synthesis. In general, an analysis of the obtained absorption and transmission spectra (insets to Fig. 8a,c) in the visible and UV range reveals that the synthesized particles exhibit significant absorption at wavelengths between 200 and 260 nm.

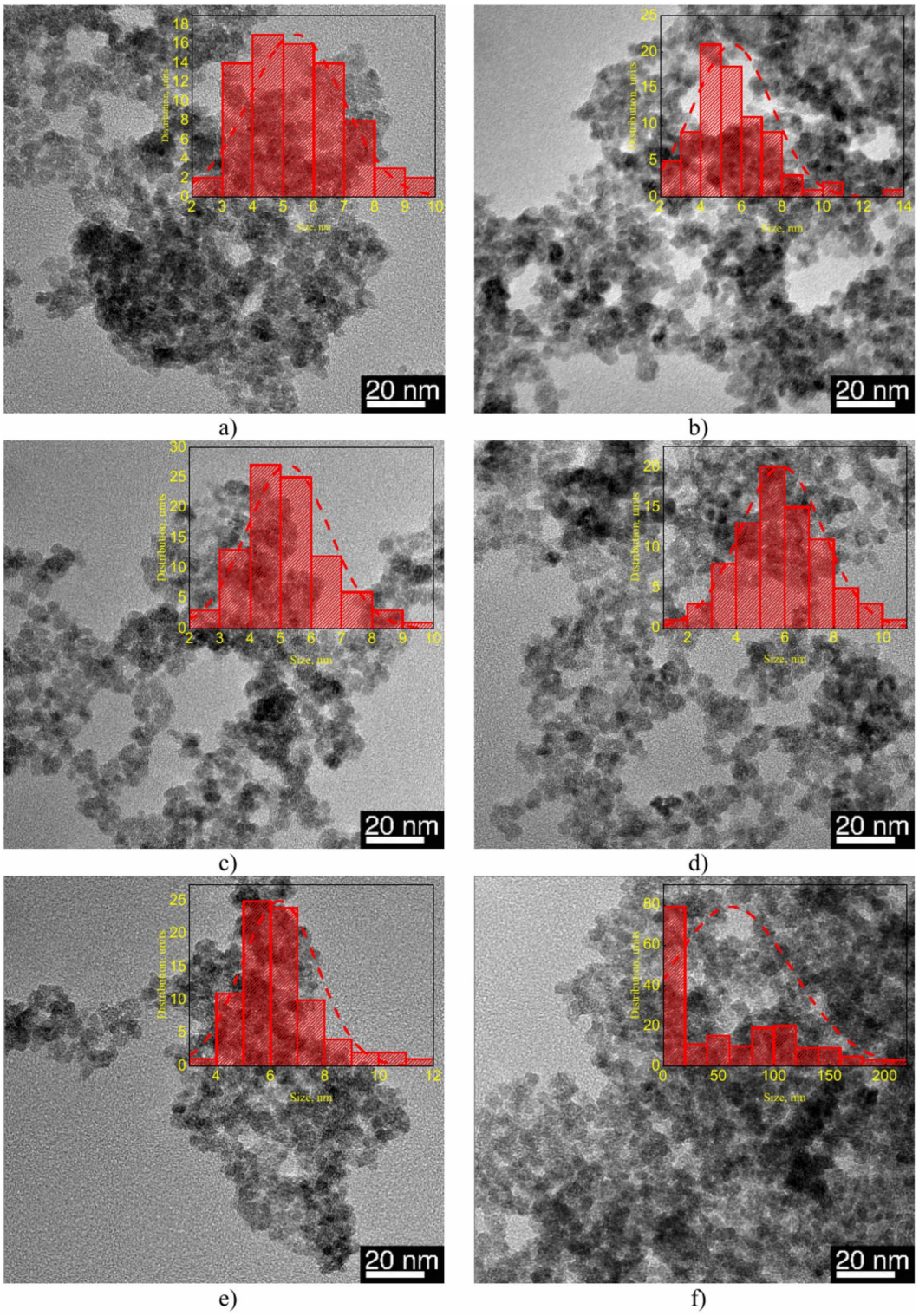

Fig. 4. TEM images of ZrO_2 particles obtained using $ZrO(NO_3)_2{\cdot}2H_2O$ by hydrothermal synthesis at temperatures (**a**–**f**) 110–160 °C.

To study the phase stability of the ZrO_2 particles, all samples were annealed at temperatures from 100 to 1000 ℃ for 2 h. Figure 9 depicts the cubic phase content percentage as a function of temperature. The data indicate that the phase composition of all synthesized particles remains stable between 100 and 500 °C. Beyond this range, however, there is a marked decrease in the cubic phase content and a corresponding increase in the monoclinic phase content. As the temperature rises above 500 ℃, particle growth and sintering of conglomerates occur, leading to the following phase transformation c-ZrO_2→m-ZrO_2. The average crystallite size calculated using

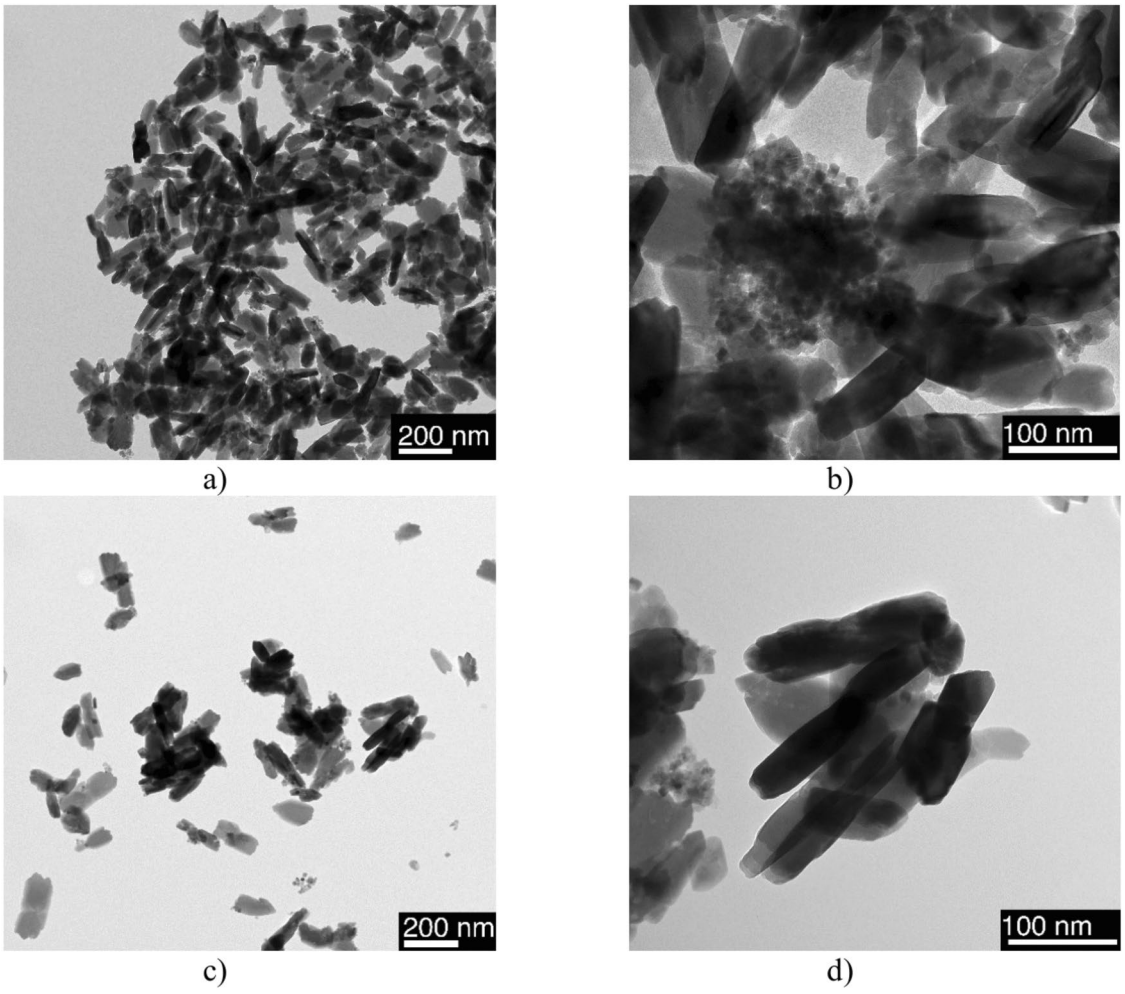

Fig. 5. TEM images of ZrO_2 particles, obtained using (**a**, **b**) $ZrOCl_2 \cdot 8H_2O$ and (**c**, **d**) $ZrO(NO_3)_2 \cdot 2H_2O$ at T = 160 °C.

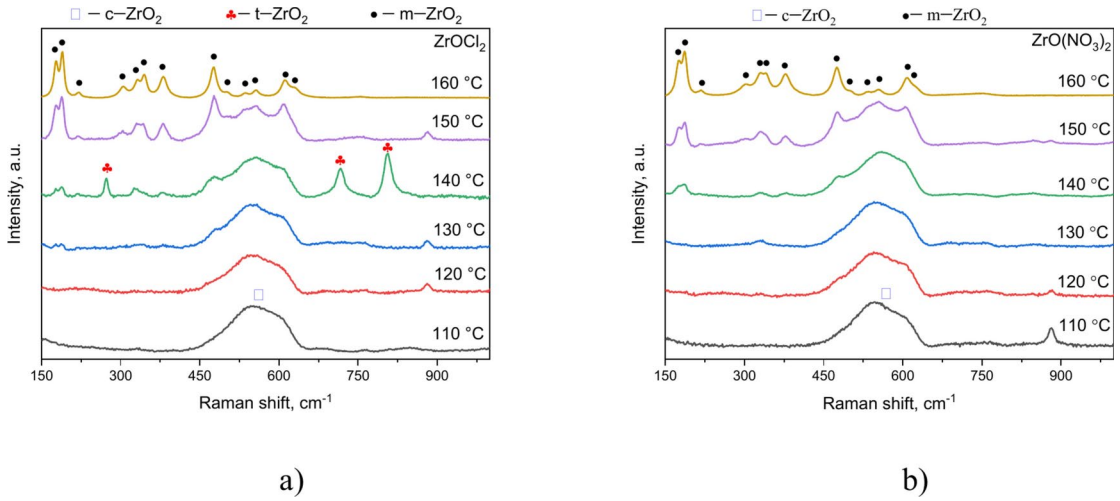

Fig. 6. Raman spectra of ZrO_2 particles prepared using (**a**) $ZrOCl_2 \cdot 8H_2O$ and (**b**) $ZrO(NO_3)_2 \cdot 2H_2O$ by hydrothermal synthesis at different temperatures.

$T_{synthesis}$ (°C)	Starting material	Zr, at. %	O, at. %	Na, at. %	Cl, at. %	N, at. %
110	$ZrOCl_2{\cdot}8H_2O$	24.9	65.7	5.5	3.9	–
	$ZrO(NO_3)_2{\cdot}2H_2O$	26.4	64.1	5.4	–	5.1
120	$ZrOCl_2{\cdot}8H_2O$	29.7	59.9	5.8	4.6	–
	$ZrO(NO_3)_2{\cdot}2H_2O$	29.6	61.8	4.1	–	4.5
130	$ZrOCl_2{\cdot}8H_2O$	28.2	62.8	5.2	3.8	–
	$ZrO(NO_3)_2{\cdot}2H_2O$	29.2	60.3	4.7	–	5.8
140	$ZrOCl_2{\cdot}8H_2O$	28.6	61.5	4.4	5.5	–
	$ZrO(NO_3)_2{\cdot}2H_2O$	27.8	62.0	4.8	–	5.4
150	$ZrOCl_2{\cdot}8H_2O$	26.6	63.7	6.5	3.2	–
	$ZrO(NO_3)_2{\cdot}2H_2O$	30.4	61.3	4.5	–	3.8
160	$ZrOCl_2{\cdot}8H_2O$	29.6	61.7	4.4	4.3	–
	$ZrO(NO_3)_2{\cdot}2H_2O$	30.9	60.2	5.2	–	3.7

Table 1. Comparison of chemical compositions of obtained samples after hydrothermal synthesis.

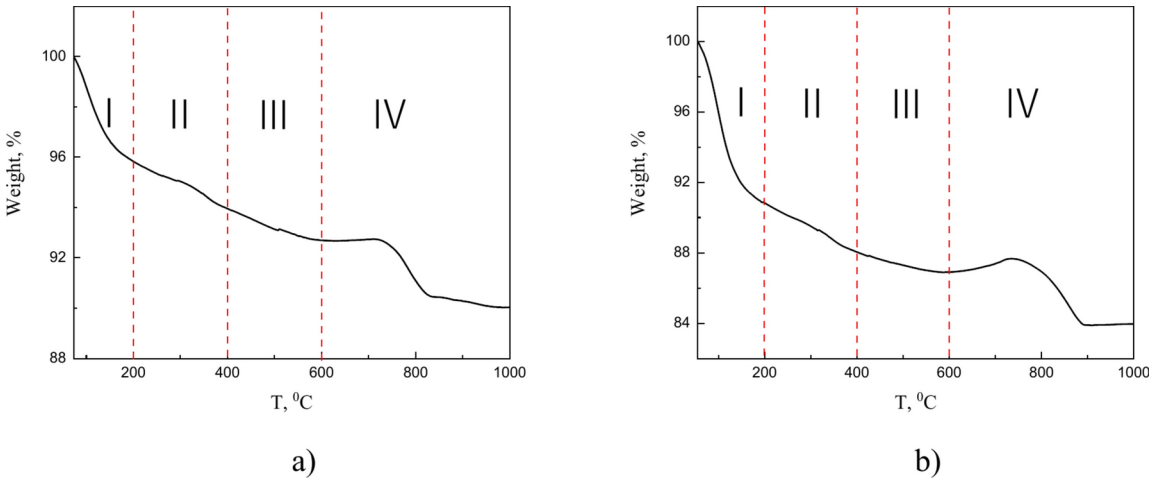

Fig. 7. TGA curves for samples synthesized at 130 ℃ using (**a**) $ZrOCl_2{\cdot}8H_2O$ and (**b**) $ZrO(NO_3)_2{\cdot}2H_2O$.

the Scherrer equation (Fig. 2) confirms the presence of particle size growth processes driven by surface energy minimization and the sintering of nanoparticle conglomerates.

Thus, the high-temperature c-ZrO_2 phase remains stable up to 600 °C. When temperature exceeds 600 ℃, a rapid phase transition from c-ZrO_2 to m-ZrO_2 occurs. The mechanism behind this transition is associated with the sintering of contacting nanoparticles and the reduction of surface energy. In the fabrication of ZrO_2-c reinforced bulk ceramics, the temperature treatment of the precursor powders should not be higher than 600 °C and good mixing of the components should be ensured to avoid aggregation of zirconia particles. Significant particle aggregation is likely to trigger the c → m transition, which diminishes the hardening effect and undermines the improvement of mechanical properties. It was also determined that the synthesized nanoparticles can be used as materials for absorbing mid-UV light (wavelength 200–260 nm).

Conclusions

In this study, ZrO_2 nanoparticles were synthesized using the hydrothermal method with various precursors and at different temperatures. X-ray diffraction revealed that at synthesis temperatures of 110–130 ℃ the obtained particles consisted exclusively of the c (t)-ZrO_2 phase with an average crystallite size of 5 nm. Further increase in the synthesis temperature resulted in larger crystallite sizes, ranging from 10 to 30 nm, which consequently induced the phase transition from c-ZrO_2 to m-ZrO_2. Investigations performed using TEM confirmed that the particle size for samples containing only c (t)-ZrO_2 phase was in the range of 4–10 nm and increased up to 10–200 nm along with the increase in the fraction of m-ZrO_2 phase in the sample. Raman spectroscopy determined that at synthesis temperatures of 110–130 °C, the nanoparticles contained the c-ZrO_2 phase, with its fraction decreasing as the synthesis temperature increased, which is consistent with the X-ray diffraction results. TGA tests indicated that the obtained ZrO_2 nanoparticles contained 14–17% of water, –OH groups and residual synthesis products (PEG and Na-containing compounds). Optical spectroscopy data demonstrated that ZrO_2 nanoparticles are highly effective at absorbing radiation in the mid-UV range (200–260 nm) and have an energy band gap of 4.8–5.1 eV. Thermal exposure tests confirmed that all samples remain stable within the temperature range of 100–500 °C. When the temperature exceeds 500 °C, the fraction of the monoclinic phase in the samples

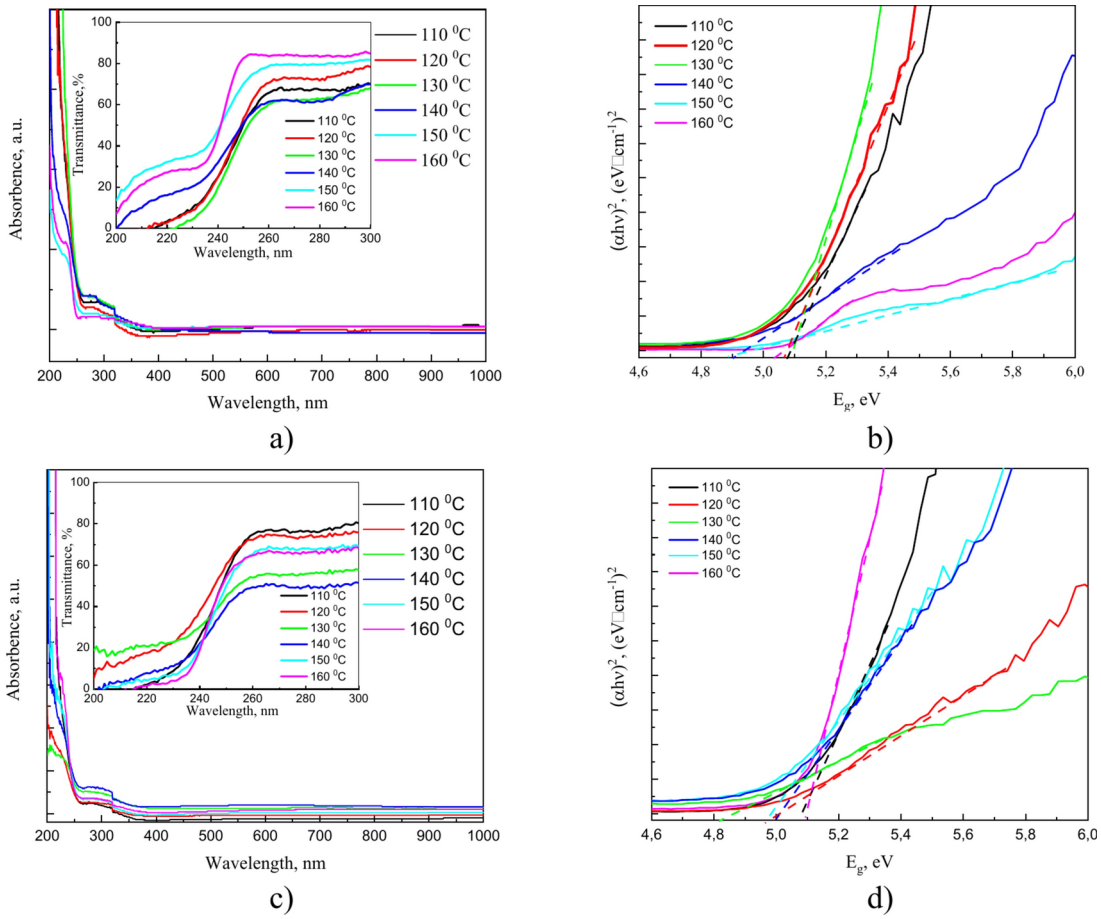

Fig. 8. Absorbance spectra and Tauc plots for samples obtained at different temperatures by hydrothermal synthesis using (**a**, **b**) $ZrOCl_2 \cdot 8H_2O$ and (**c**, **d**) $ZrO(NO_3)_2 \cdot 2H_2O$, respectively. Insets display transmission spectra in the wavelength range of 200–300 nm.

	E_g (eV)					
	110, °C	**120, °C**	**130, °C**	**140, °C**	**150, °C**	**160, °C**
$ZrOCl_2 \cdot 8H_2O$	5.08	5.07	5.09	4.91	4.89	5.03
$ZrO(NO_3)_2 \cdot 2H_2O$	5.07	4.97	4.82	4.99	4.97	5.09

Table 2. E_g values for ZrO_2 particles obtained using different precursors.

increases rapidly, which is associated with particle growth due to sintering. The synthesized nanopowders can be used as UV radiation absorbers and as hardening additives in technical ceramics.

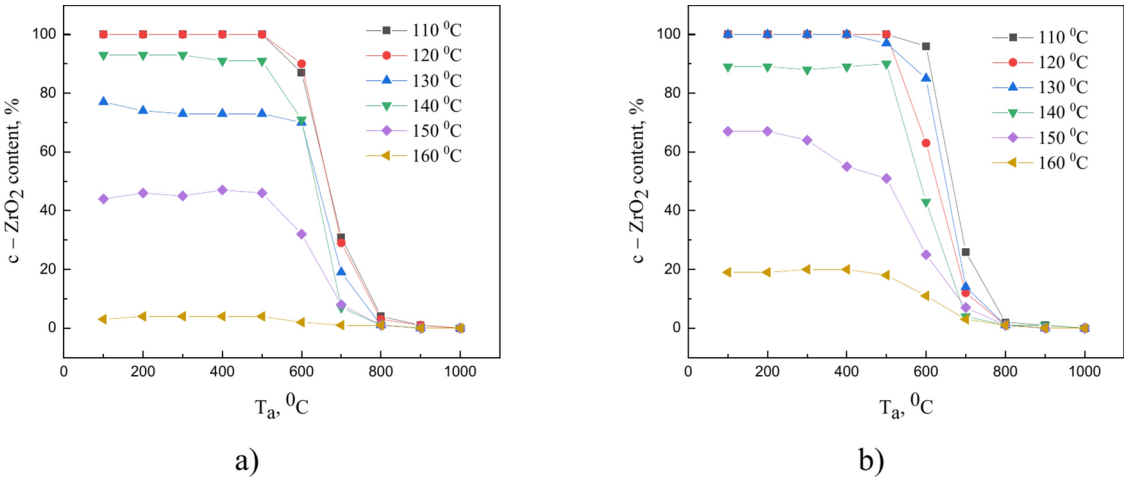

Fig. 9. Percentage of cubic phase content obtained from (**a**) $ZrOCl_2$-$8H_2O$ and (**b**) $ZrO(NO_3)_2$-$2H_2O$ at different temperatures as a function of annealing temperature.

Data availability

Data sets generated during the current study are available from the corresponding author on reasonable request.

Received: 19 August 2024; Accepted: 18 November 2024
Published online: 26 November 2024

References

1. Raj, S., Hattori, M. & Ozawa, M. Ag-doped ZrO_2 nanoparticles prepared by hydrothermal method for efficient diesel soot oxidation. *Mater. Lett.* **234**, 205–207 (2019).
2. Hidayat, D., Syoufian, A., Hasanudin, H., Utami, M. & Wijaya, K. Synthesis and application of Na2O/ZrO2 nanocomposite for microwave-assisted transesterification of castor oil. *ICS Phys. Chem.* **1**, 26 (2021).
3. Bansal, P., Kaur, N., Prakash, C. & Chaudhary, G. R. ZrO2 nanoparticles: An industrially viable, efficient and recyclable catalyst for synthesis of pharmaceutically significant xanthene derivatives. *Vacuum* **157**, 9–16 (2018).
4. Shukla, M. K., Balyan, Y., Kumar, A., Bhaskar, T. & Dhar, A. Catalytic oxidation of soot by CeO2–ZrO2 catalysts: Role of Zr. *Mater. Chem. Phys.* **286**, 126161 (2022).
5. Sathyaseelan, B. *et al.* Studies on structural and optical properties of ZrO2 nanopowder for opto-electronic applications. *J. Alloys Compd.* **694,** 556–559 (2017).
6. Chitoria, A. K., Mir, A. & Shah, M. A. A review of ZrO2 nanoparticles applications and recent advancements. *Ceram. Int.* **49**, 32343–32358 (2023).
7. Seo, J. Y., Oh, D., Kim, D. J., Kim, K. M. & Kwon, J. S. Enhanced mechanical properties of ZrO2–Al2O3 dental ceramic composites by altering Al2O3 form. *Dental Mater.* **36**, e117–e125 (2020).
8. Zahra, T. et al. Electrocatalytic water splitting studies on zirconium oxide nanoparticles synthesized by biomimetic synthesis route. *Ionics (Kiel)* **29**, 5339–5352 (2023).
9. Bruns, S., Britze, C., Vergöhl, M., Feller, A. & Meining, S. UV bandpass filters based on Ta2O5 and ZrO2 for solar observation. in *Proc. SPIE* vol. 11852, 118521P (2021).
10. Sinhamahapatra, A., Jeon, J.-P., Kang, J., Han, B. & Yu, J.-S. Oxygen-deficient zirconia (ZrO2-x): A new material for solar light absorption. *Sci. Rep.* **6**, 27218 (2016).
11. Hayashi, H., Yoshida, O. & Suzuki, H. ZnO-ZrO2 films with good UV-shielding properties prepared by a single step sol-gel method. *J. Ceram. Soc. Jpn.* **117**, 978–982 (2009).
12. Mallakpour, S. & NezamzadehEzhieh, A. Polymer nanocomposites based on modified ZrO2 NPs and poly(vinyl alcohol)/poly(vinyl pyrrolidone) blend: Optical, morphological, and thermal properties. *Polym. Plast. Technol. Eng.* **56**, 1136–1145 (2017).
13. Alin, M., Kozlovskiy, A. L., Zdorovets, M. V. & Uglov, V. V. Study of the mechanisms of the t-ZrO2 → c-ZrO2 type polymorphic transformations in ceramics as a result of irradiation with heavy Xe22+ ions. *Solid State Sci.* **123**, 106791 (2022).
14. Akhlaghi, O. et al. Transparent high-strength nanosized yttria stabilized zirconia obtained by pressure-less sintering. *J. Eur. Ceram. Soc.* **42**, 7187–7195 (2022).
15. Zhang, X. L. et al. Ultrafast hydrogenation of magnesium enabled by tetragonal ZrO2 hierarchical nanoparticles. *Mater. Today Nano* **18**, 100200 (2022).
16. Abbas, M. K. G., Ramesh, S., Tasfy, S. F. H. & Lee, K. Y. S. A state-of-the-art review on alumina toughened zirconia ceramic composites. *Mater. Today Commun.* **37**, 106964 (2023).
17. Herráez-Galindo, C., Rizo-Gorrita, M., Maza-Solano, S., Serrera-Figallo, M.-A. & Torres-Lagares, D. A review on CAD/CAM yttria-stabilized tetragonal zirconia polycrystal (Y-TZP) and polymethyl methacrylate (PMMA) and their biological behavior. *Polymers (Basel).* **14**, 906 (2022).
18. Mokhena T. C. and John, M. J. and M. M. J. and M. A. Zirconia-based nanocomposites. in *Handbook of Polymer and Ceramic Nanotechnology* (ed. Hussain Chaudhery Mustansar and Thomas, S.) 1505–1525 (Springer International Publishing, Cham, 2021). https://doi.org/10.1007/978-3-030-40513-7_47.
19. Yang, Y., Hu, C., Liu, Q. & Li, J. Research progress and prospects of colored zirconia ceramics: A review. *J. Adv. Ceram.* https://doi.org/10.26599/JAC.2024.9220941 (2024).
20. El-Amir, A. A. M., Li, S., Abdelgawad, M. & Ewais, E. M. M. MgAl2O4-reinforced c-ZrO2 ceramics prepared by spark plasma sintering. *J. Korean Ceram. Society* **58**, 574–582 (2021).
21. Maiti, T. K. et al. Zirconia- and ceria-based electrolytes for fuel cell applications: Critical advancements toward sustainable and clean energy production. *Environ. Sci. Pollut. Res.* **29**, 64489–64512 (2022).

22. Song, Y. et al. Preparation and mechanical properties of zirconia ceramics doped with different Y2O3 contents. *J. Wuhan Univ. Technol.-Mater. Sci.* **38**, 1287–1292 (2023).
23. Bruni, Y. L., Garrido, L. B. & Aglietti, E. F. Properties of CaO-ZrO2 based composites. *Procedia Mater. Sci.* **8**, 203–210 (2015).
24. Giniyatova, S. G. *et al.* Investigation of the phase composition, structural, mechanical, and dielectric properties of (1−x)·ZrO2-x·CeO2 ceramics synthesized by the solid-state method. *Appl. Sci.* **14**, 2663 (2024).
25. Varshney, M., Sharma, A., Chae, K. H., Kumar, S. & Won, S. O. Electronic structure and dielectric properties of ZrO2-CeO2 mixed oxides. *J. Phys. Chem. Solids* **119**, 242–250 (2018).
26. Basu, B. Toughening of Y-stabilized tetragonal zirconia ceramics. *Int. Mater. Rev.* **50**, 239–256 (2005).
27. Liu, S. *et al.* Tetragonal nanosized zirconia: hydrothermal synthesis and its performance as a promising ceramic reinforcement. *Inorganics (Basel)* **11**, 217 (2023).
28. Yang, C. et al. Modified hydrothermal treatment route for high-yield preparation of nanosized ZrO2. *Ceram. Int.* **46**, 19807–19814 (2020).
29. Sigwadi, R., Mokrani, T. & Dhlamini, M. The synthesis, characterization and electrochemical study of zirconia oxide nanoparticles for fuel cell application. *Physica B Condens. Matter.* **581**, 411842 (2020).
30. Shukla, S. & Seal, S. Mechanisms of room temperature metastable tetragonal phase stabilisation in zirconia. *Int. Mater. Rev.* **50**, 45–64 (2005).
31. Mosavari, M., Khajehhaghverdi, A. & Mehdinavaz Aghdam, R. Nano-ZrO2: A review on synthesis methodologies. *Inorg. Chem. Commun.* **157**, 111293 (2023).
32. Tran, T. V. et al. Green synthesis of ZrO2 nanoparticles and nanocomposites for biomedical and environmental applications: A review. *Environ. Chem. Lett.* **20**, 1309–1331 (2022).
33. Mohsen, Q. et al. Effect of pH on hydrothermal synthesis of ZrO2 nanoparticles and their electrocatalytic activity for hydrogen production. *Int. J. Electrochem. Sci.* **17**, 22073 (2022).
34. Song, X. et al. Thermophysical and mechanical properties of cubic, tetragonal and monoclinic ZrO2. *J. Mater. Res. Technol.* **23**, 648–655 (2023).
35. Dudnik, E. V. Modern methods for hydrothermal synthesis of ZrO2-based nanocrystalline powders. *Powder Metall. Metal Ceram.* **48**, 238–248 (2009).
36. Noh, H. J., Seo, D. S., Kim, H. & Lee, J. K. Synthesis and crystallization of anisotropic shaped ZrO2 nanocrystalline powders by hydrothermal process. *Mater. Lett.* **57**, 2425–2431 (2003).
37. Deshmane, V. G. & Adewuyi, Y. G. Synthesis of thermally stable, high surface area, nanocrystalline mesoporous tetragonal zirconium dioxide (ZrO2): Effects of different process parameters. *Microporous Mesoporous Mater.* **148**, 88–100 (2012).
38. Liu, L., Wang, S., Zhang, B., Jiang, G. & Yang, J. Supercritical hydrothermal synthesis of nano-ZrO2: Influence of technological parameters and mechanism. *J. Alloys Compd.* **898**, 162878 (2022).
39. Behbahani, A., Rowshanzamir, S. & Esmaeilifar, A. Hydrothermal synthesis of zirconia nanoparticles from commercial zirconia. *Procedia Eng.* **42**, 908–917 (2012).
40. Li, C. et al. Effect of reaction temperature on crystallization of nanocrystalline zirconia synthesized by microwave-hydrothermal process. *J. Alloys Compd.* **561**, 23–27 (2013).
41. Szepesi, C. J. & Adair, J. H. High yield hydrothermal synthesis of nano-scale zirconia and YTZP. *J. Am. Ceram. Society* **94**, 4239–4246 (2011).
42. Toraya, H., Yoshimura, M. & Somiya, S. Calibration curve for quantitative analysis of the monoclinic-tetragonal ZrO2 system by X-ray diffraction. *J. Am. Ceram. Society.* **67**, C-119–C−121 (1984).
43. Horti, N. C., Kamatagi, M. D., Nataraj, S. K., Wari, M. N. & Inamdar, S. R. Structural and optical properties of zirconium oxide (ZrO2) nanoparticles: Effect of calcination temperature. *Nano Express* **1**, 10022 (2020).
44. Kolen'ko, Y.V., et al. Physicochemical properties of nanocrystalline zirconia hydrothermally synthesized from zirconyl chloride and zirconyl nitrate aqueous solutions. *Zhurnal Neorganicheskoj Khimii* **49**, 1237–1242 (2004).
45. Giniyatova, S. G. *et al.* Structural, dielectric, and mechanical properties of high-content cubic zirconia ceramics obtained via solid-state synthesis. *Appl. Sci.* **13**, 10989 (2023).
46. Broström, M., Enestam, S., Backman, R. & Mäkelä, K. Condensation in the KCl–NaCl system. *Fuel Process. Technol.* **105**, 142–148 (2013).
47. Peymani, R., Poursalehi, R. & Yourdkhani, A. Optical and structural properties of colloidal zirconia nanoparticles prepared by arc discharge in liquid. in *AIP Conference Proceedings*. 1920 (2018).

Author contributions

Conceptualization, Y.G, R.S., N.V., D.S., M.Z., D.B. and A.K.; methodology, Y.G., R.S., N.V., D.S., M.Z., D.B. and A.K.; formal analysis, Y.G., R.S., N.V., D.S., M.Z., D.B. and A.K.; investigation, Y.G., R.S., N.V., D.S., M.Z., D.B. and A.K.; resources, A.K.; writing—original draft preparation, review, and editing, Y.G, R.S. and N.V.; visualization, A.K. and Y.G.; supervision, A.K.

Funding

This research was funded by the Science Committee of the Ministry of Education and Science of the Republic of Kazakhstan (No. BR21882390).

Declarations

Competing interests

The authors declare no competing interests.

Additional information

Correspondence and requests for materials should be addressed to Y.G.

Reprints and permissions information is available at www.nature.com/reprints.

Publisher's note Springer Nature remains neutral with regard to jurisdictional claims in published maps and institutional affiliations.